Engineering Structures 172 (2018) 334–345

Contents lists available at ScienceDirect

Engineering Structures

journal homepage: www.elsevier.com/locate/engstruct

Sensitivity and uncertainty analysis of AAR affected reinforced concrete shear walls

Mohammad Amin Hariri-Ardebili, Victor E. Saouma*

Department of Civil Environmental and Architectural Engineering, University of Colorado, Boulder, CO 80305, USA
X-Elastica, LLC, Boulder, CO 80303, USA

ARTICLE INFO

Keywords:
Concrete
Alkali silica reaction
Degradation
Finite element
Shear wall
Random properties

ABSTRACT

Whereas many publications report on alkali aggregate reaction (AAR) expansion or test analyses, very few address the more pressing issue of its impact on structures. Furthermore, given the uncertainties associated with characterization of the material, probabilistic based approach are not known to have been reported in the literature. This paper addresses these limitations through an analysis of a reinforced shear wall. A two-prone approach is followed: first a sensitivity analysis is performed to narrow the number of random variables (RVs) to the most relevant ones. Then, an uncertainty quantification is performed through Latin Hypercube Sampling with and without AAR expansion. Then the capacity curves (including the summarized ones to 16, 50 and 84% fractiles) are developed. Probability of non-exceedance of a specific capacity (i.e., limit state) is shown though the so-called fragility curves. It is found that in some cases AAR increases the shear capacity, while in others it decreased it. It highly depends on the initial combination of the RVs.

1. Introduction

Increasingly engineers are confronted with the need to perform predictive structural assessment based on limited or incomplete data set. This may include damage up to failure assessment (in the context of so-called performance based engineering), or round robin benchmarks. As such deterministic analyses are of limited predictive values, and a stochastic analysis is warranted.

This paper focuses on the development of a methodology for such assessment, and is believed to be the first such contribution in the context of structural failure following alkali aggregate reaction (AAR) (or alkali silica reaction – ASR) induced expansion. As a vehicle for such an application, analysis of a previously tested concrete reinforced shear wall is performed.

In light of this potential problem which may affect numerous nuclear containment vessel structures (NCVS), various research projects were put in place. The Department of Energy (DOE) is sponsoring large scale mockup tests to assess the effect of confinement on AAR expansion [1]. The Nuclear Regulatory Commission (NRC) has entered into an inter-agency agreement with the National Institute of Science and Technology (NIST) to conduct a multi-million dollars research program on the structural performance of nuclear power plants (NPP) affected by AAR [2]. NRC is also funding a grant and cooperative agreement with the University of Colorado to assess the effect of AAR on the shear strength deterioration, and for the integrity assessment of a NCVS suffering from AAR subjected to seismic loading [3]. Furthermore, Nextera has funded a major research program at the University of Texas to assess the effect of AAR on the shear strength of concrete specimen [4]. Similar effort have been undertaken abroad. Most notably in Canada through funding from the Canadian Nuclear Safety Commission (CNSC) where shear wall affected by AAR have been tested (and whose analyses are reported below) [5]. Finally, a major project on the same theme was recently initiated in France through support from the Institut de Radioprotection et de Sûreté Nucléaire (IRSN) [6].

In terms of related numerical simulations, the authors have investigated the shear response of nuclear containment panels [7], and thus this work constitutes a natural extension of past analyses combined with the separately developed methodology for probabilistic assessment [8,9].

Surprisingly, very few publications address the impact of AAR on the response of an engineering structure (i.e. not a laboratory specimen) through a finite element analysis. Most of the effort at the structural level seems to have been limited on the analyses of dams [10–14]. Fewer publications address the impact of AAR on containment structures. Takatura et al. [15] and Chénier et al. [16] investigated containment structures affected by AAR in Japan and Canada respectively. Again there is a limited number of publications reporting the structural analysis of bridges [17–20] or massive reinforced concrete structures

* Corresponding author at: Department of Civil Environmental and Architectural Engineering, University of Colorado, Boulder, CO 80305, USA.
E-mail address: saouma@colorado.edu (V.E. Saouma).

https://doi.org/10.1016/j.engstruct.2018.05.115
Received 7 February 2018; Received in revised form 24 April 2018; Accepted 30 May 2018

[21]. However, many researchers have focused their attention to merely analyze laboratory tests such as [22]. As to the nonlinear finite element analysis of reinforced concrete shear walls, there is a wide set of literature [23–26].

1.1. Objective

Through the auspices of the Organization for the Economic Cooperation and Development (OECD), a project for the Assessment of Structures subject to Concrete Pathologies (ASCET) was setup with one of its objectives being the organization of a blind simulation benchmark to predict the behavior of structural elements with AAR. The selected structure to be modeled was a reinforced concrete shear wall with AAR and subjected to reverse cyclic load. The wall had been tested at the University of Toronto [27]. Participants were given the opportunity to calibrate their models through the first phase (I) of the project where experimental data after eight months was made available, and asked to submit their numerical prediction for the wall responses (with and without AAR) after thirty months of swelling.

This paper will detail the advanced analysis performed, and focus will be placed on its main contribution: casting an AAR analysis (notoriously plagued by large uncertainties) within a probabilistic framework.

2. Test description

The tested shear wall is shown in Fig. 1, as well as the location of LVDTs (which measure the displacement between the bottom of the upper beam and the top of the lower beam). Detailed dimensions of the shear wall itself as well as two columns and two beams are illustrated in Fig. 2. Reinforcement distribution is also shown in this figure. The 10 M and 20 M reinforcements have cross-sectional areas of 100 and 200 mm^2, yield stresses of 430 and 465 MPa, and elastic moduli of 182,000 and 190,000 MPa, respectively. In the experiment, a constant vertical force of 800 kN is applied through a 2″ thick steel plate, and the wall is subjected to a reverse cyclic pushover displacement (not to be confused with a seismic load). The bottom beam is anchored to the strong floor.

A total of three walls were cast, one without AAR (SW) and two others with AAR (SW-260 and SW-1000). The first two (one with and the other without AAR) were tested about 260 days (one of them was tested couple of days earlier) after casting, and the results made available for calibration. The third wall was tested about 1000 days after casting and participants in the benchmark round robin were asked to make predictions. The reported mechanical properties for the concrete at 260 days are: 79.0/63.7 MPa for f'_c, 4.76/3.24 MPa for f'_t, 179.3/120.2 N/m for G_F, and 47,150/35,750 MPa for E.

Results of the tests are summarized in Fig. 3. It should be noted that the peak loads with (SW-260) and without AAR (SW) expansion are 1354 and 1180, or 14% difference. This is a relatively small change, and given the uncertainties in measurement that difference may not be entirely attributed to the effect of expansion.

As no creep data was made available, and in light of the relative young age of the tested specimens, creep was ignored. On the other hand, based on simple “engineering judgment”, it was apparent that potential bond loss at the juncture between column and base had to be addressed. This could be done by either wrapping joint elements (with hard to define characteristics) around the rebars at this location, or approximately by reducing the cross-sectional area of the steel at that location. This reduced cross-section will trigger large plastic deformation (akin of the ones induced by debonding) before the other segments yield.

3. Modeling approach

In performing the numerical simulation of an experimental test, one must recognize that four possibilities are present:

1. An inconsequential analysis where results are simply to meet basic engineering common sense expectations.
2. *Post-mortem* simulation where one has the luxury to fine-tune/calibrate a model until near exact results are obtained (which is nearly always possible, irrespective of the model accuracy).
3. Predictive analysis for the future response of a structure.
4. Blind simulation benchmark of an experimental test. However, it should be noted that there are two major sources of uncertainties:

- Experimental: How accurately was the test performed?, how credible are the results?, are the reported results sufficiently clear and unambiguous?, and is it the model or the test that is being checked?
- Numerical: Can one perform a single deterministic and predictive analysis, or wouldn’t a probabilistic-based analysis be more appropriate given the epistemic nature of the uncertainties?

The current benchmark study does allow calibration (level 2 above) and requires prediction of known results (level 4). As to the two level of uncertainties (experimental and numerical), those are separately addressed below prior to the analyses results.

3.1. Uncertainties

Experimental: Though experimental uncertainties (accuracy and precision) are inherent in any test program, this benchmark exercise suffered from the additional pitfall of limited and incomplete data.[1] This made the exercise quite intractable problem, if it was to be handled in detail, and as a (partial) remedy a stochastic analysis is reported.

Epistemic: Simply put, epistemic uncertainties are those caused by an incomplete knowledge of the exact material properties [29].

3.2. Study objectives

Given that a nonlinear constitutive model for concrete contains numerous variables, most of which not provided or even measurable, a two prone approach should be followed:

Sensitivity Analysis: To determine which of the many random variables in the shear wall model are most sensitive.

Uncertainty Analysis: After selection of the most sensitive random variables, perform a Monte Carlo Simulation to provide a probabilistic estimate of the prediction.

This approach was recently followed by the authors for the analysis of a major bridge suffering from AAR [20].

4. Data preparation

The analysis hinges on two constitutive models: one for the concrete nonlinearity (a fracture-plasticity smeared crack model) [30], and the other for the AAR [21]. Both have been implemented in the authors finite element code Merlin [31], and most importantly validated in accordance with the RILEM TC 259 report [32].

4.1. Concrete smeared crack model

The concrete constitutive model was a fracture plasticity model [30] implemented as a so-called smeared crack model. As most constitutive models, this one has a number of parameters and not all can be directly measured experimentally. Hence, some are assigned values based on other calibrations or experience. This will invariably lead to

[1] During the ensuing meeting, it was evident that boundary conditions assigned lead to many differing assumptions, and only one set of load displacement was given to participants.

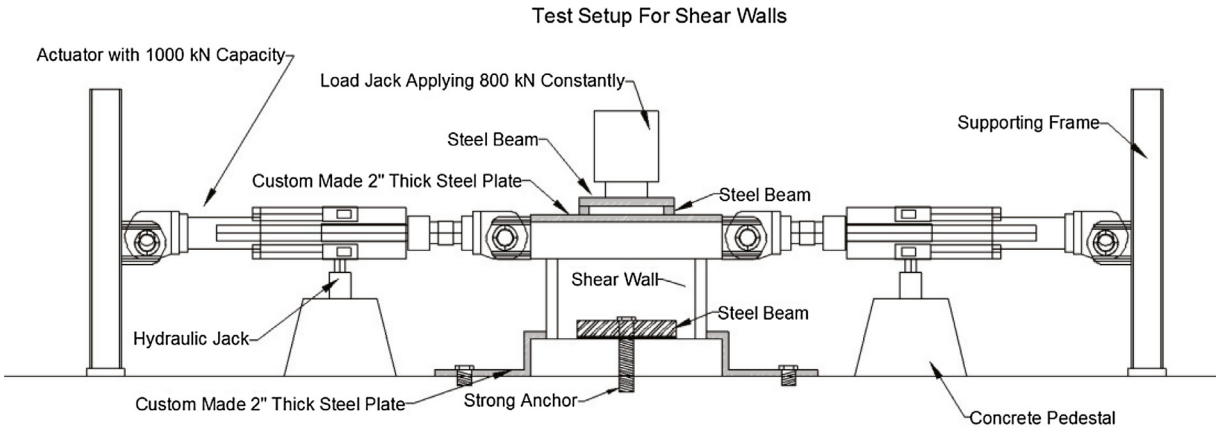

(a) Full test set up

(b) Photo of shear wall inside the actuator (c) Instrumentation; LVDT

Fig. 1. Test setup for the shear wall [27,28].

uncertainties, and as such can be treated as random variables. Table 1 lists the 12 identified variables including: (a) mean values, (b) authors best estimates for the coefficients of variation, (c) lower and upper bonds for uncertainty quantification, and (d) minimum-maximum ones for the sensitivity analysis. The fourth and fifth columns show the activation or deactivation of the variables in sensitivity and uncertainty analyses (1: active, 0: de-active).

In all analyses, random variables are assumed to have a normal distributional model (though a log-normal may have been more suited for some variables) with mean and coefficients of variations (COV) shown in the table. However, those values were subsequently adjusted since the distribution was truncated, Fig. 4. One should note that the normal distribution has maximum entropy over the real numbers with a specified variance, i.e., a particular moment [33]. It should be emphasized that reported values are the authors best estimates in the context of this proposed analysis, and what some may perceive as incorrect values should not detract attention from the objective of this study. Furthermore, the range for the sensitivity analysis is different from the one for uncertainty quantification. In the former it is set to 50% of the mean (unless it is constrained by the constitutive model), this choice is dictated by a need to accentuate impact of RVs on the Tornado Diagram. In the second it is fixed to 20% of the mean value in all random variables.

4.2. Reinforcement and bond-slip

The material properties for the reinforcement (either in web and columns or in the beams) were shown in Section 2. Though reinforcement properties exhibit little if any epistemic uncertainty, the approach taken was to reduce the area of the reinforcement crossing the beam-column (or beam-web) intersection to account for possible bond-slip. As such, the cross-sectional area was arbitrarily reduced by 20% and treated as the only steel random variable in the uncertainty quantification.

4.3. AAR expansion

4.3.1. Model

Proper modeling of the AAR expansion is of paramount importance to this study, and as such has received great scrutiny. The adopted AAR model is described in Appendix A, where the kinetics of the expansion is given by Eq. (A.1) and (A.3), while the degradation in Eq. (A.4). Those two equations define what will be the variables associated withe the uncertainty quantification (they were not considered in the sensitivity analysis):

- τ_L Latency time, Eq. (A.1) and (A.3)
- τ_C Characteristic time, Eq. (A.1) and (A.3)
- ε^{∞} Maximum AAR expansion, Eq. (A.1)
- U_L Activation energy of the latency time, Eq. (A.3)
- U_C Activation energy of the characteristic time, Eq. (A.3)
- β_E Residual elastic modulus at the end of the reaction, Eq. (A.4)
- β_{ft} Residual tensile strength at the end of the reaction, Eq. (A.4)

Warning: It should be emphasized that whereas in this exercise the entire wall will be assigned the same expansion as the one observed from laboratory specimens, this is not exactly valid. There is ample evidence in the literature that actual structural expansions are (in most cases) much lower than those determined from laboratory prisms (due to different ambient conditions and ensuing leaching). This issue has

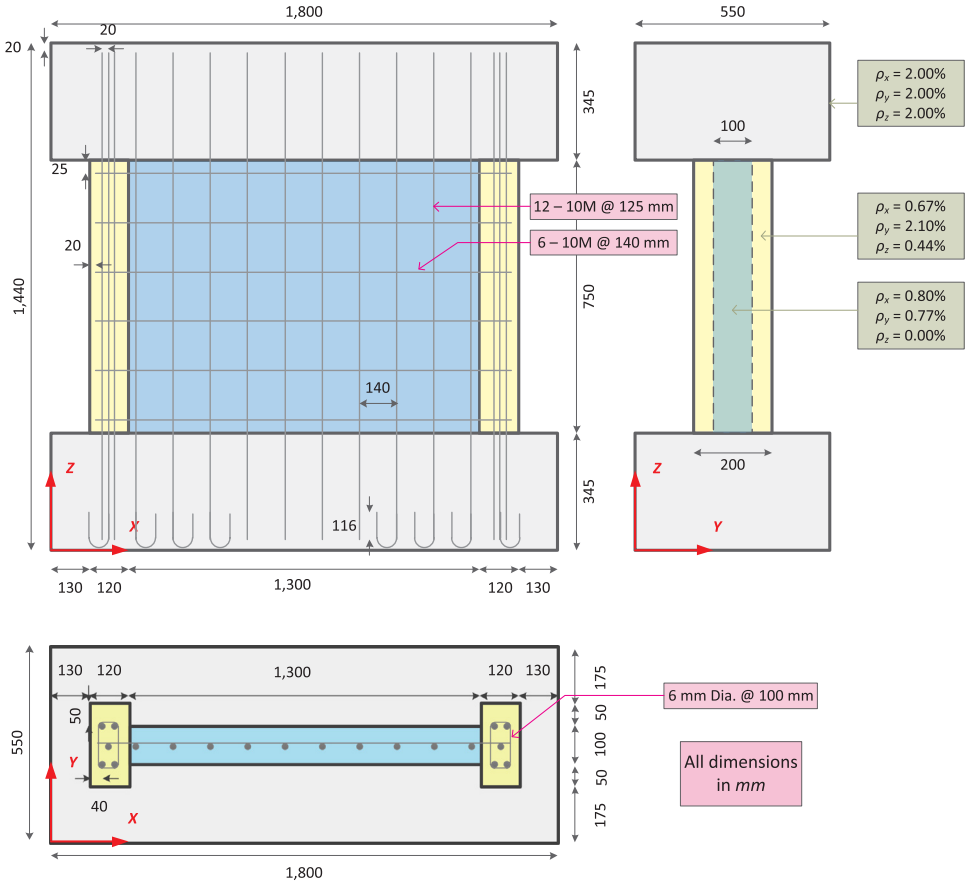

Fig. 2. Dimensions of the shear wall, beams, columns and the reinforcement distribution.

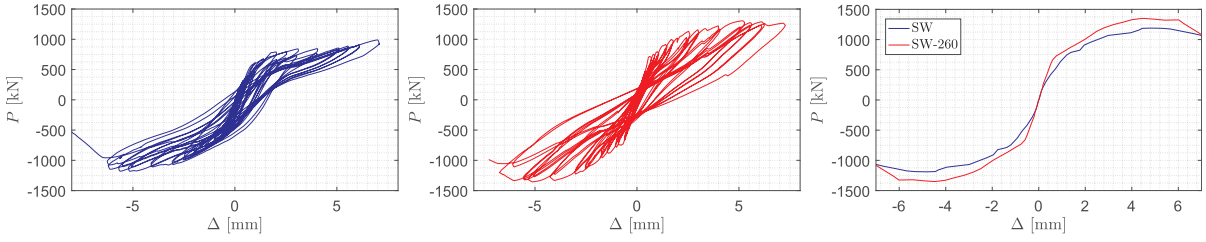

Fig. 3. Force displacement results for the first set of walls after 8 months, adapted from [27].

been partially addressed by Leemann and Merz [34], Fournier et al. [35], Lindgård et al. [36], [37], Ideker et al. [38]. Furthermore, and despite the (relatively) small size of the walls, material heterogeneity would imply that one cannot *strictu sensus* apply the same AAR property throughout the wall without an attempt to use some homogenization techniques in the spirit of [39]. Those two problems were not addressed in the reported analysis, as the added complication could have hampered the primary focus of this contribution: applicability of a stochastic approach for AAR modeling.

4.3.2. Parameter identification

Data for expansion over the first 260 days was available (from experiment), as well as the corresponding degraded tensile strength and elastic modulus (see Section 2).

t = 260 days: In Fig. 5, the reported expansions for SW and SW-260 (longitudinal and transverse) in Orbovic et al. [5] are shown. The indicated points, while not exactly matching the ones reported by experiment; however, they are sufficiently close to be retained.

A simple Matlab code was developed to fit a curve (based on Eq. (A.2)) to the reported experimental time-expansion values. As a result, the following parameters were obtained: $\tau_c = 81$ days, $\tau_l = 61$ days, and $\varepsilon^{\infty} = 0.00223$ (0.22%). It should be noted that the concrete expansion at 260 days is relatively small.

t = 1000 days: Determination of the AAR key parameters at 1000 days is more problematic and values will be extrapolated from the current one with a margin of uncertainty. With reference to Fig. 6(a), expansion up to ~250 days is known, and we need to guesstimate the one at time $t = 1000$ days.

Kinetics: It was assumed that the expansion at that time will obey a uniform distributional model ranging from a minimum 0.25% and a maximum of 0.45%. Then, using a Latin Hypercube sampling (LHS) technique, 100 curves are fitted between those points. The corresponding 100 values of τ_l and τ_c are shown in Fig. 6(b) where the zero values of τ_l are associated with those expansion with a quasi-linear early expansion.

Deterioration: E and f_t' at time t_0 and t_{260} are given. Using these values a normal distribution model is assumed with the reported values as mean, and a COV reported in Table 1. Then, based on Eq. (A.4) and

Table 1
Material parameters used in numerical simulations.

Characteristics	Symbol	Unit	SA	UQ	Mean	COV_{UQ}	$[LB, UB]_{UQ}$	$[min, max]_{SA}$
Smeared crack model								
Mass density	ρ	Gg/m^3	0	0	0.00244	–	–	–
Thermal expansion coefficient	α	1/°C	0	0	9.9e−6	–	–	–
Modulus of elasticity[a]	E	MPa	1	1	47,150	0.2	[28,290 66,010]	[23,575 70,725]
Poisson's ratio	ν	–	0	0	0.2	–	–	–
Tensile strength[a]	f_t	MPa	1	1	4.76	0.2	[2.86, 6.66]	[2.38, 7.14]
Exponential softening[a]	G_F	MN/m	1	1	1.79e−4	0.2	[1.08e−4, 2.51e−4]	[8.95e−5, 2.68e−4]
Compressive strength[a]	f_c	MPa	1	1	−79.0	0.2	[−110.6, −47.4]	[−118.5, −39.5]
Compressive critical displacement	w_d	m	1	0	−5e−4	–	–	[−7.5e−4, −2.5e−4]
Factor for return direction	β	–	1	0	0.50	–	–	[0.25, 1.0]
Factor for roundness of failure surface	e	–	1	0	0.55	–	–	[0.5, 1.0]
Onset of nonlinearity in compression	f_{c0}	MPa	1	0	−20	–	–	[−30, −10]
Plastic strain at compressive strength	ϵ_{cp}	–	1	0	−1e−3	–	–	[−2e−3, −5e−4]
Reinforcement								
Yield stress of main rebar (vertical and horizontal)	f_y^R	MPa	1	0	430	–	–	[215, 645]
Yield stress of main stirrups	f_y^S	MPa	1	0	430	–	–	[215, 645]
Yield stress of crossing rebar	f_y^{R-Cr}	MPa	1	0	430	–	–	[215, 645]
Modulus of elasticity of crossing rebar	E^{R-Cr}	MPa	1	0	182,000	–	–	[91000, 273000]
Cross sectional area of crossing rebar	A_r^{R-Cr}	m^2	1	1	8e−5	0.2	[4.8e−5, 1e−4]	[6e−5, 1e−4]

[a] Reported values from experiments; SA: sensitivity analysis; UQ: uncertainty quantification; LB: lower bound; UB: upper bound.

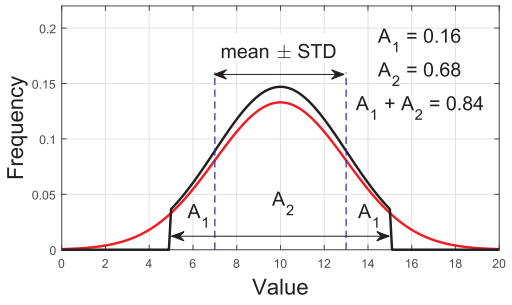

Fig. 4. Truncation of normal distribution model and bounds.

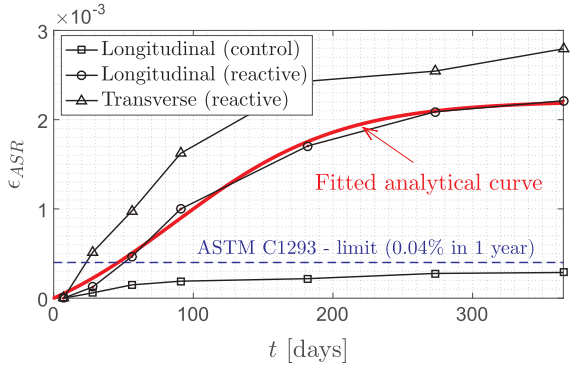

Fig. 5. Reported expansion from [5] and corresponding fitted analytical curve.

the set of 100 values of τ_l and τ_c, degradation curves are obtained, Fig. 7.

5. Finite element model

The prepared finite element mesh, shown in Fig. 8(a) and (b), consists of quadrilateral elements. There are three layers of elements in the web and five layers in the columns. Top and bottom beams are assumed to be linear elastic while the columns and web have the smeared crack model parameters. Over all, there are 1240 solid elements in the model. All the elements in the web and the columns are cubic, while those in the beams do not have a regular pattern. This is due selection of optimal mesh size in the beam (larger elements than the web and column) and does not affect the results since the beam is linear elastic.

The bottom beam is fixed at the base and the sides. The incremental displacement is applied on the left side of the top beam. Moreover, there is a traction on the upper face of top beam, Fig. 8(c). Note that the applied boundary conditions are based on our understanding of the tests. As later found, the base beam may allow the slippage with respect to the support (i.e. strong floor), and hence the adopted model for numerical simulation is too rigid. The reported cyclic load is identical to the one shown in Fig. 8(d). Each load cyclic is applied though 10 increments.

6. Results

Results will be presented as follows:

1. Deterministic analysis of SW and SW-260, followed by calibration.
2. Sensitivity analysis of SW.
3. Uncertainty quantification of SW and SW-1000 along with probability of non-exceedance of a specific shear wall capacity.

6.1. Deterministic analysis and calibration

In this first set of analyses, the meshes shown in Fig. 8 and mean values from Table 1 are used for the SW and SW-260. The preliminary envelope for SW was obtained (not shown here) and it is evident that the numerical response is too stiff, and an adjustment has to be made. In light of the experimental uncertainties addressed in Section 3.1 and the assumed rigid supports, this discrepancy is attributed to "slack" in the system and an adjustment is to be made. Thus, and in the spirit of this benchmark where calibration is indeed expected first, the displacements were simply multiplied by 2.3 resulting in a shift of the results which closely matched the experimental results. Indeed, the final report of the Benchmark workshop concluded (among other things), [40] that

> *The wall measurements were not sufficiently documented. A single measurement of the displacement of the upper beam is not enough to calibrate numerical models. Simulated displacements are lower than measured displacements in all simulations and based on numerical*

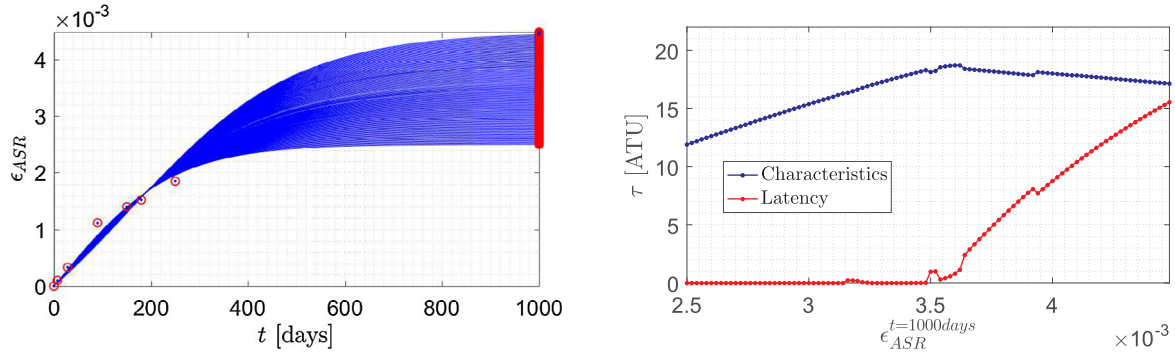

(a) Expansion curve (b) Predicted τ values

Fig. 6. Optimization-based curve fitting to find the future expansion.

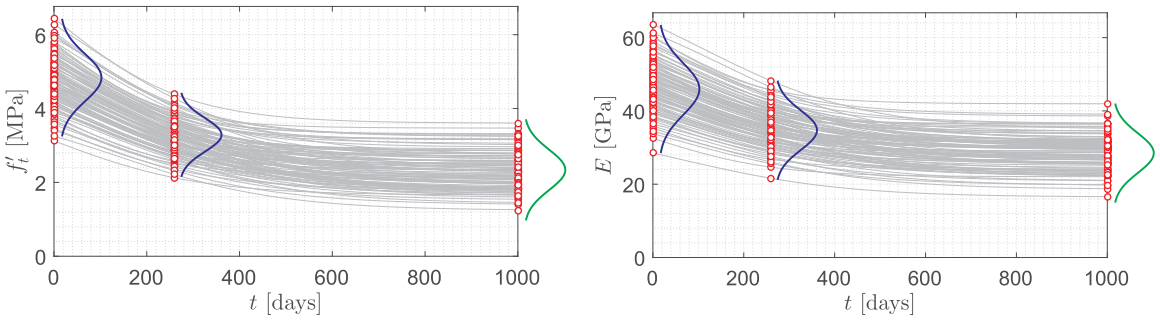

(a) f_t' (b) E

Fig. 7. Estimation of residual coefficients.

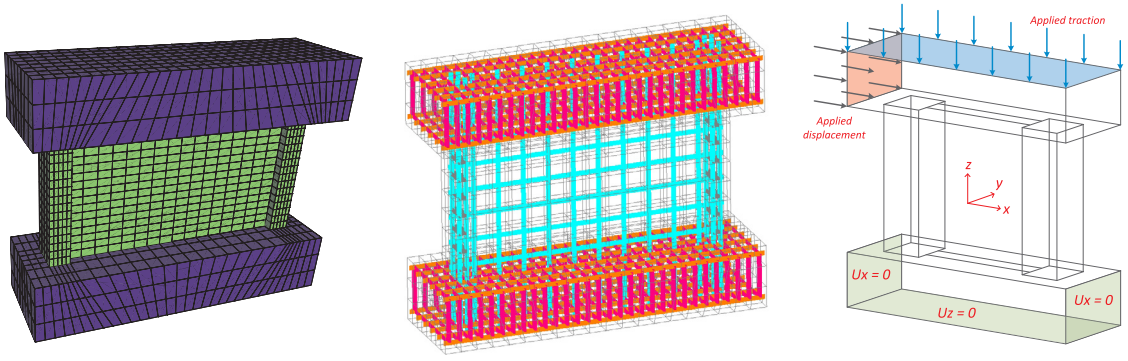

(a) Finite element mesh (b) Reinforcement (c) Boundary conditions

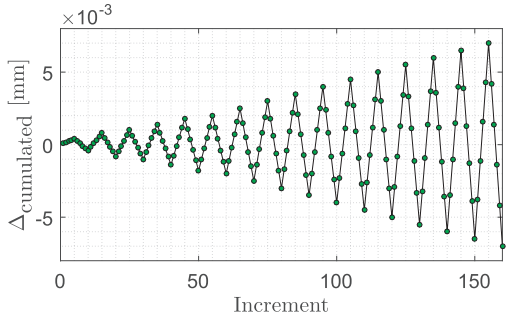

(d) Reversed cyclic loading and increments

Fig. 8. Finite element model, boundary condition and loading.

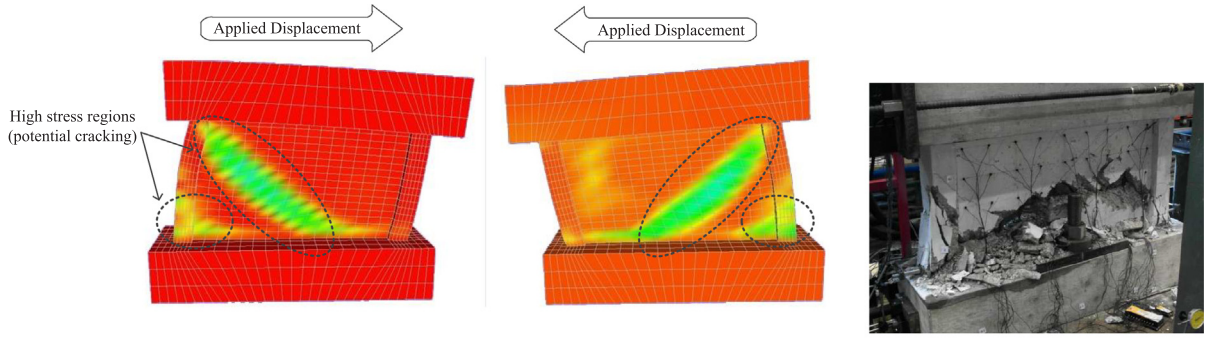

(a) Deformed shapes; Contour shows the maximum principal strains (b) Observed failure [41]

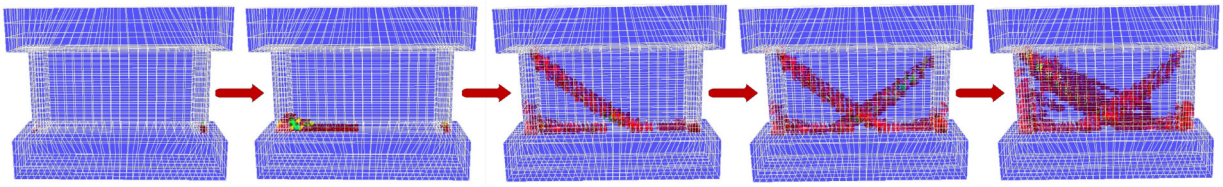

(c) Crack propagation under reverse loading (first rightward, then leftward)

Fig. 9. Structural response of shear wall under cyclic displacement (without ASR) [41].

simulations, the wall boundary conditions have more important impact on wall displacements than the constitutive laws.

Hence, from this point onward, all numerical results will be subjected to this calibration factor. Then, the results of SW-260 were compared, Fig. 12 and again, the two curves are nearly identical. For illustrative purpose, the deformed shape with maximum principal stresses are shown in Fig. 9(a), and the evolution of the accompanying (smeared) cracks is finally shown in Fig. 9(c). As seen, the regions with high principal stresses correlate well with the computed failure path; both are in good agreement with the observed failure mode from the test. Visual inspection of these plots provides a graphical confirmation of the reliability of the analysis.

6.2. Sensitivity analyses

The sensitivity analysis procedure is rooted in the Taylor's Series-Finite Difference Estimation described in Appendix B. In the context of this analysis, $n = 15$ random variables identified in Table 1 are retained, thus a total of $2n + 1 = 31$ analyses are performed. First the capacity curves [42] of all the analyses are obtained, Fig. 10(a). It is noted that the experimental curve does indeed fall within the range of results, and that in some cases there is an early failure characterized by a sudden drop in the post-peak load carrying curve (whereas some softening resulting from induced displacements would have been expected). Then the sensitivities are sorted and results shown in the format of a so-called Tornado diagram [43], Fig. 10(b).

From this figure, it was determined that the steel reinforcement whose crossing the beam-wall interface plays a prominent role in the response through the yield stress and cross-sectional area. As to the concrete, the predominant variables affecting the shear wall carrying capacity are: the compressive strength, plastic strain at compressive failure, modulus of elasticity are amongst the major factors influencing the response. The least important variables are the yield stress of the stirrups and onset of concrete nonlinearity in compression, and concrete compressive critical displacement. Concrete tensile strength and fracture energy are among the intermediary sensitive variables.

It should be emphasized that though the Tornado diagram gives an indication of the response sensitivity to the variables, not all of them are actually random. For instance, the uncertainty in the steel material properties is smaller than that in concrete, and thus for simplicity and practical purposes, it is not treated as a random variable.

6.3. Uncertainty quantification

Uncertainty quantification has retained the variables listed in

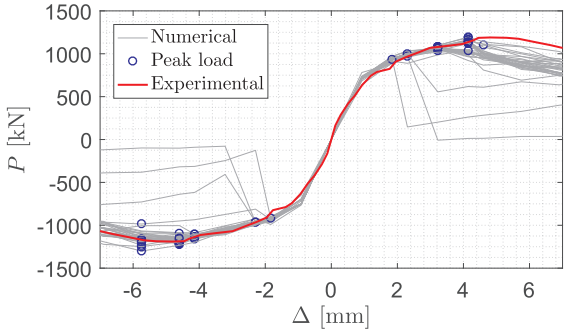

(a) Capacity curves

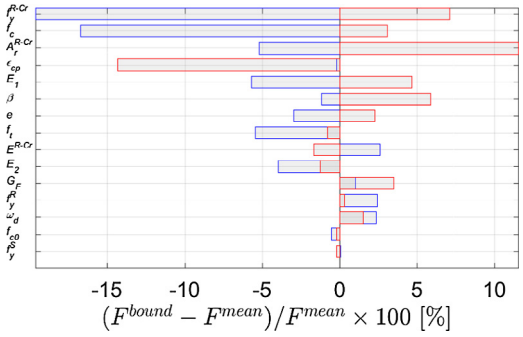

(b) Tornado diagram

Fig. 10. Results of sensitivity analysis on concrete constitutive model.

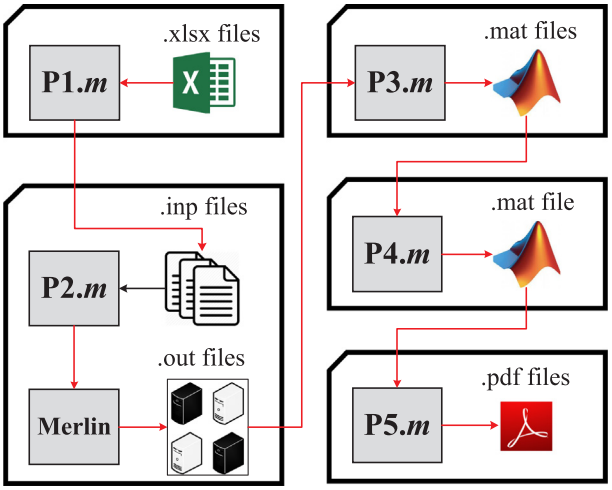

Fig. 11. File generation and automation algorithm.

Table 1 (column 5) as random with a normal distributional model. Selection of those are based on the Tornado diagram and engineering common sense. Since there is no solid information about the inter-correlation among the random variables, it is assumed that they are independent. This is one of the limitations of the study which may affect the dispersion of the results [9].

6.3.1. Automation of probabilistic analysis

Given the complexity in data manipulation from input data definition, random variable selection, generation of finite element meshes, execution, data mining to extract results, and plotting key diagrams an automated procedure was set up. This was accomplished through a Matlab [44] based set of sequential programs `P1.m`, `P2.m`, `P3.m`, `P4.m` and `P5.m` whose inter-connectivity is illustrated in Fig. 11.

`p1.m` reads the user specified variables, probability distribution models, ranges, and correlation coefficients, and then generates N_{sim} (in this study 100) input files. Those in turn are executed through `p2.m` which calls the finite element code Merlin. Next, the results are individually extracted from 100 output files and stored as binary files using `p3.m`. Results are further consolidated into a single data-base using `p4.m`. Finally, `p5.m` extracts the results from the database and generates the desired plots. For each output parameter, results are plotted along with their mean, 16% and 84% fractiles ranges (which correspond to minus and plus one standard deviation in a log-normal distributional model).

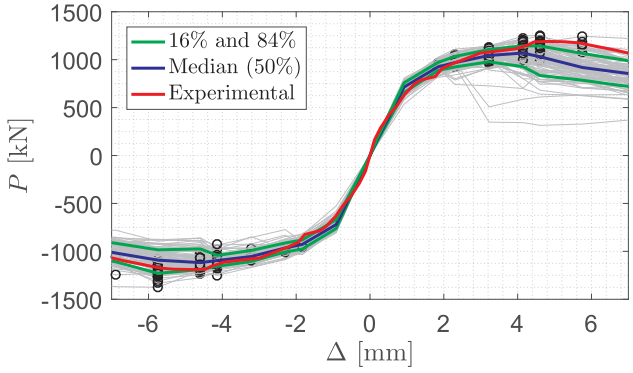

Fig. 12. Results of uncertainty quantification on capacity curves in SW-260.

6.3.2. Prediction

Following completion of the 100 analyses (it should be noted that five analyses did not converge most likely due to an unfavorable set of AAR material parameters), `P5.m` generated the capacity curves for SW. Then, the 16% and 84% fractile curves are sought. This is simply achieved by sweeping through the full range of displacements, and for each one identify the points below which 16% and 84% of the load fall. The capacity curves for SW, Fig. 12, is in close agreement with the experimental data. However, contrarily to the first sensitivity analysis, the uncertainty one shows that the experimental tests fall within the 16% and 84% fractiles. Finally, we reach the objective of this study which is to provide a probabilistic-based assessment of the shear wall capacity when tested 1000 days after casting. This will be shown later in Section 6.4.

Results warrant additional examination to fully grasp the structural responses. As such, Fig. 13(a) plots the shear wall capacity for SW and SW-1000 along with the corresponding histograms and probability distribution function. Fig. 13(b) shows the cumulative distribution functions (CDF) for empirical (dashed lines) and fitted (continuous lines based on log-normal assumption) for both SW and SW-1000. Mean and logarithmic standard deviation are 1.14 MN and 0.090 MN for SW, and 1.13 MN and 0.11 MN for SW-1000 respectively. It should be noted that there is higher standard deviation in SW-1000 as there are more RVs. Moreover, note that in ~60% of the analyses, the shear capacity was reduced by the pre-existence of AAR, and in ~40% it increased. Finally, the point in which the CDF rotates from SW to SW-1000 is located at probability of 0.65.

Last by not least, a similar scheme where AAR may increase or reduce the shear strength capacity was observed by the authors in a separate study [7], shown in Fig. 14. The monotonic shear strength of a panel was numerically determined with and without initial AAR expansion. In both cases, the initial stiffness was reduced by AAR.

Regretfully, it was not possible to clearly identify the set of parameters which cause an increase (or decrease) in shear strength capacity due to previous AAR. It is speculated that the increased in strength is associated with a particularly unfavorable combination of variables (not necessarily reflecting a likely physical scenario) randomly selected by the Latin Hypercube Simulation. However, this remains an open question of the utmost importance which requires further in depth study.

6.4. Comparison with experimental results

Following the submission of blind prediction, the organizers provided the results of the three tests (one at 260 days used for calibration by participants) and two others performed at 1000 days (expansion to be predicted). Whereas SW-260 includes all 15 cycles, SW-1000 does not report all of them. Hence, without the benefit of all cycles, it is impossible to clearly and unequivocally compare force and displacement with great accuracy. Finally, and most importantly the comparison between reported experimental results and blind numerical prediction is plotted in Fig. 15 which shows a good correlation between the prediction and measurements. One of the experimental tests (B1) exhibits two sudden large cycles at the end which can be associated with the global failure of the wall.

7. Conclusions

Originally motivated by a participation in a Round-Robin predictive study of the load carrying capacity of a shear wall affected by AAR, the authors have broadened their analysis into a stochastic one. The viability of a two pronged approach to the prediction of an AAR affected complex structure was proven. The combination of a sensitivity analysis followed by uncertainty quantification, proved to be ideal tools for a stochastic analysis of a structure.

In the narrower context of the shear wall, facilitated by the nearly

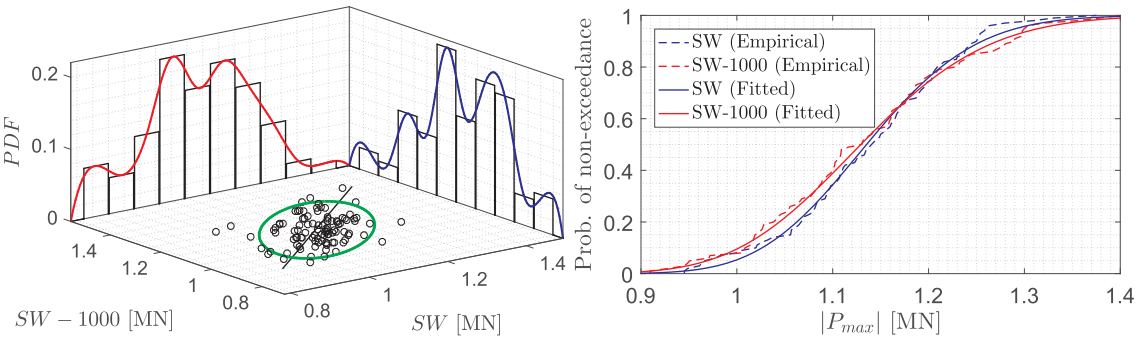

(a) Individual peak points and histograms (b) Cummulative density function

Fig. 13. Comparison of SW and SW-1000 models.

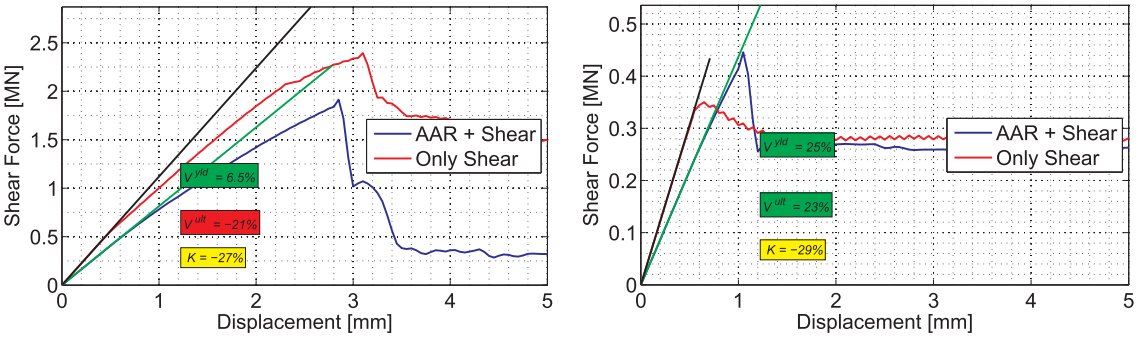

(a) Shear capacity reduction (b) Shear capacity increase

Fig. 14. Impact of AAR on shear capacity of concrete panels from a NCVS [7].

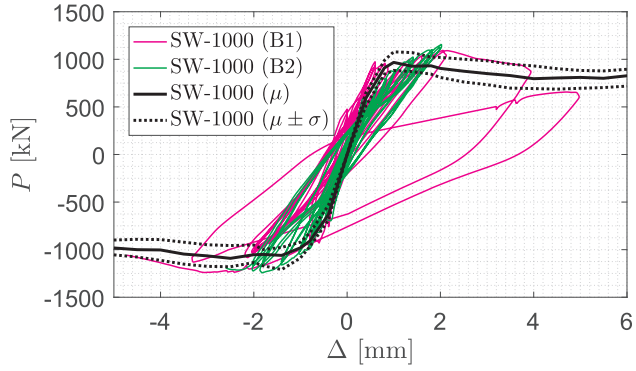

Fig. 15. Comparison between blind numerical prediction (mean and ± standard deviation) and experimental tests at 1000 days (two tests) adapted from [40].

identical expansions at 260 and 1000 days, good prediction was achieved. However, and this could only be highlighted from the multiple analyses needed by the stochastic model, it was found that in some cases the AAR increased the shear resistance, while in others it decreased it. Within the scope of this study, it was impossible to identify the combination of variables leading to either one of the two cases.

Finally, though the shear wall analysis is only applicable to an internal structural element in a nuclear power plant, conceptually it may elucidate better understanding of the response of the NCVS. As AAR is unlikely to affect the structural integrity of the NCVS by itself, it is very likely to affect the shear resistance under a seismic excitation. This interaction of AAR and seismic excitation, within the context of a deterministic and stochastic analyses is the subject of development by the authors through a grant from the NRC.

Acknowledgments

The authors would like to acknowledge the financial support of the U.S. Nuclear Regulatory Commission (Madhumita Sircar Technical Analyst) to the University of Colorado (Boulder), Grant No. NRC-HQ-60-14-G-0010. The valuable information provided by the benchmark organizers, Mr. Orbovic and Nevander is gratefully acknowledged.

Appendix A. AAR constitutive model

The theoretical underpinning of the AAR model used in this paper has been presented by the authors separately, [45,21]. It will be briefly reviewed. The AAR expansion is considered to be a volumetric one, which rate is given by the following function

$$\dot{\varepsilon}_V^{AAR}(t,\theta,RH) = \Gamma_t(f_t'|w_c,\sigma_I|COD_{max})\,\Gamma_c(\overline{\sigma},f_c')g(RH)\,\dot{\xi}(t,\theta)\,\varepsilon^{\infty}|_{\theta=\theta_0} \tag{A.1}$$

where ε^{∞} is the final volumetric expansion as determined from laboratory tests at temperature θ_0. $0 \leqslant \Gamma_t \leqslant 1$ is a parameter which reduces the expansion in the presence of large tensile stresses (macro-cracks absorbing the gel), f_t' the tensile strength, and σ_I the major (tensile) principal stress. Similarly, $0 \leqslant \Gamma_c \leqslant 1$ is a parameter which accounts for the absorption of the gel due to compressive induced stresses, $\overline{\sigma}$ and f_c' are the hydrostatic stress, and the compressive strength of the concrete, respectively. $0 \leqslant g(RH) \leqslant 1$ is a function of the relative humidity (set to zero if the humidity is below 80%), $\dot{\xi}(t,\theta)$ the kinetics law given by

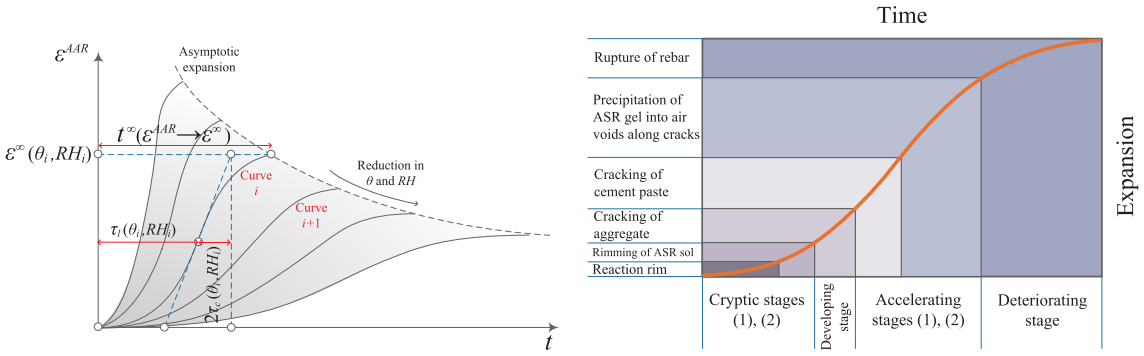

(a) Effect of temperature and relative humidity (b) Physical interpretation

Fig. A.16. AAR expansion curve [54].

$$\xi(t,\theta)=\frac{1-\exp\left(-\frac{t}{\tau_c(\theta)}\right)}{1+\exp\left(-\frac{(t-\tau_l(\theta))}{\tau_c(\theta)}\right)} \tag{A.2}$$

where τ_l and τ_c are the latency and characteristic times, respectively. The former corresponds to the inflexion point, and the latter is defined in terms of the intersection of the tangent at τ_l with the asymptotic unit value of ξ, Fig. A.16(a). They are given by

$$\begin{aligned}\tau_l(\theta)&=\tau_l(\theta_0)\exp\left[U_l\left(\tfrac{1}{\theta}-\tfrac{1}{\theta_0}\right)\right]\\ \tau_c(\theta)&=\tau_c(\theta_0)\exp\left[U_c\left(\tfrac{1}{\theta}-\tfrac{1}{\theta_0}\right)\right]\end{aligned} \tag{A.3}$$

expressed in terms of the absolute temperature ($\theta^oK=273+T^oC$) and the corresponding activation energies. U_l and U_c are the activation energies, minimum energy required to trigger the reaction for the latency and characteristic times, respectively. Once the volumetric AAR strain is determined, it is decomposed into a tensorial strain in accordance to the three weight factors associated with the principal stresses. Finally, degradation of the tensile strength and elastic modulus is accounted for as follows:

$$\begin{aligned}E(t,\theta)&=E_0\left[1-(1-\beta_E)\xi(t,\theta)\right]\\ f_t(t,\theta)&=f_{t,0}\left[1-(1-\beta_{f_t})\xi(t,\theta)\right]\end{aligned} \tag{A.4}$$

The model is relatively simple to implement in an existing finite element code and has been implemented in many finite element codes Pian et al. [46], El Mohandes and Vecchio [47], Rodriguez et al. [48], Pan et al. [49], Huang and Spencer [50], Huang et al. [51], Ben-Ftima et al. [52].

In the context of this study, there are no good estimate for: (1) what would be the ultimate AAR induced strain as possibly determined from reliable laboratory residual expansion (not a simple task); and (2) what is the internal relative humidity in the box girder ($g(RH)$ in Eq. (A.1)). Indeed, it has long been recognized that for AAR to occur, RH must be above a certain threshold [53].

The effect of temperature and relative humidity on the kinetics of the reaction is illustrated by Fig. A.16(a) where the decrease in RH, results in a decrease of peak AAR while a in temperature will slow the reaction. Finally, The engineering significance of the (sigmoid) expansion is illustrated in Fig. A.16(b) [54].

Appendix B. Taylor's series-finite difference estimation

The concept behind the sensitivity analysis is rooted in the so-called Taylor's series finite difference estimation of the mean μ in terms of all the random variables individual means μ_i is the mean for all random variables [55]. Hence, for an independent random variables, the variance is given by

$$\mu_F=F(\mu_i) \tag{B.1}$$

where

$$Var(F)=\sigma_F^2=\sum\left(\frac{\partial F}{\partial x_i}\sigma_i\right)^2 \tag{B.2}$$

$$\frac{\partial F}{\partial x_i}\approx\frac{F_i^+-F_i^-}{2\sigma_i} \tag{B.3}$$

$$F_i^+=F(\mu_1,\ ...,\mu_i+\sigma_i,\ ...,\mu_n) \tag{B.4}$$

$$F_i^-=F(\mu_1,\ ...,\mu_i-\sigma_i,\ ...,\mu_n) \tag{B.5}$$

where σ_i are the standard deviations of the variables. Hence,

$$\sigma_F=\sum\left(\frac{F_i^+-F_i^-}{2}\right) \tag{B.6}$$

The procedure can be summarized as follows:

1. Perform an initial analysis in which all variables are set equal to their mean value. This analysis provides the mean μ.
2. Perform $2n$ analysis, in which all variables are set equal to their mean values, except variable i, which assumes a value equal to $\mu_i + \sigma_i$, and then $\mu_i - \sigma_i$.
3. For each pair of analysis in which variable x_i is modified, determine the standard deviation component associated with the specific variable i, which will provide an indication of the *sensitivity* of the results to variation of this particular variable. $\left(\frac{F_i^+ - F_i^-}{2}\right)$.
4. The standard deviation of the entire structure is then determined by simply adding all the $\left(\frac{F_i^+ - F_i^-}{2}\right)$ terms.
5. Sort the results in an descending order and form the so-called “Tornado diagram”.

This simplified method has been first reported by Benjamin and Cornell [56] in the context of structural engineering, and then used in [57–59].

References

[1] Le Pape Y, Ma Z, Cabage J, Lenarduzzi R. Design of a large-scale concrete mockup to study the effects of alkali-silica reaction on expansion, damage and shear fracture propagation in stress-confined safety related structures. Tech. Rep. Technical Report M3LW-14OR-0403012 – Rev. 1. Light Water Reactor Sustainability Program; 2014.

[2] NRC-NIST Project. Structural Performance of Nuclear Power Plant (NPP) Concrete Structures Affected by Alkali-Silica Reaction (ASR). Tech. Rep. Interagency Agreement No. NRC-HQ-60-14-I-0004; 2014. URL < https://www.nrc.gov/docs/ML1414/ML14147A221.pdf > .

[3] NRC-CU Grant. Experimental and Numerical Investigation of Alkali Silica Reaction in Nuclear Reactors. Tech. Rep. Grant and Cooperative Agreement NRC-HQ-60-14-G-0010; 2014. URL < https://www.nrc.gov/docs/ML1427/ML14274A265.pdf > .

[4] ML121160422. Impact of Alkali Silica Reaction on Seabrook Concrete Structure. Tech. Rep. ML121160422. NextEra; 2012.

[5] Orbovic N, Panesar D, Sheikh S, Vecchio F, Lamarche C, Blahoianu A. Alkali aggregate reaction in nuclear concrete structures: Part 1: a holistic approach. In: Proceedings of the 23rd conference on structural mechanics in reactor technology (SMiRT23); 2015. URL < https://www.researchgate.net/profile/Nebojsa_Orbovic2/publication/281064845_Alkali_Aggregate_Reaction_in_Nuclear_Concrete_Structures_Part_1_A_Holistic_Approach/links/55d32fae08ae7fb244f5818b.pdf > .

[6] Marquié C. IRSN R&D on Concrete Pathologies Issues: The ODOBA Project; 2016. URL < https://www.nrc.gov/public-involve/conference-symposia/ric/past/2016/docs/abstracts/marquiec-t7-hv.pdf > .

[7] Saouma V, Hariri-Ardebili M, Le Pape Y, Balaji R. Effect of alkali–silica reaction on the shear strength of reinforced concrete structural members. A numerical and statistical study. Nucl Eng Des 2016;310:295–310.

[8] Hariri-Ardebili MA, Saouma V. Probabilistic seismic demand model and optimal intensity measure for concrete dams. Struct Saf 2016;59:67–85.

[9] Hariri-Ardebili MA, Saouma VE. Sensitivity and uncertainty quantification of the cohesive crack model. Eng Fract Mech 2016;155:18–35.

[10] Léger P, Côte P, Tinawi R. Finite element analysis of concrete swelling due to alkali-aggregate reactions in dams. Comput Struct 1996;60(4):601–11.

[11] Saouma V, Perotti L, Shimpo T. Stress analysis of concrete structures subjected to alkali-aggregate reactions. ACI Struct J 2007;104:532–41.

[12] Comi C, Fedele R, Perego U. A chemo-thermo-damage model for the analysis of concrete dams affected by alkali-silica reaction. Mech Mater 2009;41:210–30.

[13] Sellier A, Bourdarot E, Multon S, Cyr M, Grimal E. Combination of structural monitoring and laboratory tests for assessment of alkali-aggregate reaction swelling: application to gate structure dam. Mater J 2009;106(3):281–90.

[14] Pan J, Xu Y, Jin F, Zhang C. A unified approach for long-term behavior and seismic response of AAR-affected concrete dams. Soil Dyn Earthquake Eng 2014;63:193–202.

[15] Takatura T, Ishikawa T, Matsumoto N, Mitsuki S, Takiguchi K, Masuda Y. Investigation of the expanded value of turbine generator foundation affected by alkali-silica reaction. In: 18th international conference on structural mechanics in reactor technology (SMIRT 18), Beijing, China, sMIRT18-H03-7; 2005. p. 2061–8.

[16] Chénier J, Komljenovic D, Gocevski V, Picard S, Chrétien G. An approach regarding aging management program for concrete containment structure at the gentilly-2 nuclear power plant. In: Proceedings of 33rd annual conference of the Canadian Nuclear Society, TCU Place, Saskatoon, Saskatchewan, Canada, vol. 1013; 2012. p. 126.

[17] Li K, Coussy O. Concrete ASR degradation: from material modeling to structure assessment. Concr Sci Eng 2002;4(13):35–46.

[18] Omikrine M, Kchakech B, Lavaud S, Godart B. A new model for the analysis of the structural/mechanical performance of concrete structures affected by DEF–Case study of an existing viaduct. Struct Concr.

[19] Wojslaw K, Wisniewski M. Nonlinear and time dependent analysis of a concrete bridge suffering from alkali–silica reaction: a case study of the Elgeseter Bridge in Trondheim [Master’s thesis]. Norwegian University of Science and Technology, Institutt for konstruksjonsteknikk; 2014.

[20] Hariri-Ardebili MA, Saouma VE, Merz C. Risk-informed condition assessment of a bridge with alkali-aggregate reaction. ACI Struct J 2018;115(2):475–87.

[21] Saouma V. Numerical modeling of AAR. CRC Press; 2014.

[22] Multon S, Seignol J-F, Toutlemonde F. Structural behavior of concrete beams affected by alkali-silica reaction. Mater J 2005;102(2):67–76.

[23] Damoni C, Belletti B, Esposito R. Numerical prediction of the response of a squat shear wall subjected to monotonic loading. Eur J Environ Civ Eng 2014;18(7):754–69.

[24] Massone LM. Strength prediction of squat structural walls via calibration of a shear–flexure interaction model. Eng Struct 2010;32(4):922–32.

[25] Koutromanos I, Stavridis A, Shing P, Willam K. Numerical modeling of masonry-infilled RC frames subjected to seismic loads. Comput Struct 2011;89:1026–37.

[26] Gattesco N, Amadio C, Bedon C. Experimental and numerical study on the shear behavior of stone masonry walls strengthened with GFRP reinforced mortar coating and steel-cord reinforced repointing. Eng Struct 2015;90:143–57.

[27] Habibi F, Sheikh S, Orbovic N, Panesar D, Vecchio F. Alkali aggregate reaction in nuclear concrete structures: Part 3: structural shear wall elements. In: Proceedings of the 23rd conference on structural mechanics in reactor technology (SMiRT23); 2015.

[28] Sheikh S. Personal Communication, March 10, 2017; 2017.

[29] Der-Kiureghian A, Ditlevsen O. Aleatory or epistemic? Does it matter? Struct Saf 2009;31:105–12.

[30] Cervenka J, Papanikolaou V. Three dimensional combined fracture-plastic material model for concrete. Int J Plast 2008;24(12):2192–220.

[31] Saouma V, Červenka J, Reich R. Merlin finite element user’s manual; 2010. < http://civil.colorado.edu/saouma/pdf/Software/users.pdf > .

[32] Saouma V, Sellier A, Multon S, Le Pape Y, Hariri-Ardebili M. Benchmark problems for AAR FEA code validation; 2017. < http://www.rilem.org/global/gene/doc_link.php?doc=2016161048_rilem-tc-259-isr-wg2-benchmark.pdf > .

[33] Hariri-Ardebili MA, Pourkamali-Anaraki F. Simplified reliability analysis of multi hazard risk in gravity dams via machine learning techniques. Arch Civ Mech Eng 2018;18(2):592–610.

[34] Leemann A, Merz C. An attempt to validate the ultra-accelerated microbar and the concrete performance test with the degree of AAR-induced damage observed in concrete structures. Cem Concr Res 2013;49:29–37.

[35] Fournier B, Ideker JH, Folliard K, Thomas M, Nkinamubanzi P, Chevrier R. Effect of environmental conditions on expansion in concrete due to alkali–silica reaction (ASR). Mater Charact 2009;60(7):669–79.

[36] Lindgård J, Nixon PJ, Borchers I, Schouenborg B, Wigum BJ, Haugen M, et al. The EU PARTNER Project-European standard tests to prevent alkali reactions in aggregates: final results and recommendations. Cem Concr Res 2010;40(4):611–35.

[37] Lindgård J, Andiç-Çakır Ö, Fernandes I, Rønning TF, Thomas MD. Alkali–silica reactions (ASR): literature review on parameters influencing laboratory performance testing. Cem Concr Res 2012;42(2):223–43.

[38] Ideker J, Bentivegna A, Folliard K, Juenger M. Do current laboratory test methods accurately predict alkali-silica reactivity? ACI Mater J 109(4).

[39] Xu X, Graham-Brady L. A stochastic computational method for evaluation of global and local behavior of random elastic media. Comput Methods Appl Mech Eng 2005;194(42):4362–85.

[40] Nevander O, Orbovic N. ASCET phase II – summary, conclusions and recommendation. Tech. Rep. OECD Nuclear Energy Agency (NEA), draft final report; 2017.

[41] Jurcut A-C. Modelling of alkali-aggregate reaction effects in reinforced concrete structures [Master’s thesis]. University of Toronto (Canada); 2015.

[42] Hariri-Ardebili M, Saouma V. Single and multi-hazard capacity functions for concrete dams. Soil Dyn Earthquake Eng 2017;101:234–49.

[43] Lee T, Mosalam K. Probabilistic seismic evaluation of reinforced concrete structural components and systems. Tech. Rep. 2006/04. Pacific Earthquake Engineering Research Center; 2006.

[44] MATLAB, version 9.1 (R2016b). Natick, Massachusetts: The MathWorks Inc.; 2016.

[45] Saouma V, Perotti L. Constitutive model for alkali aggregate reactions. ACI Mater J 2006;103(3):194–202.

[46] Pian J, Feng Y, Wang J, Sun C, Zhang C, Owen D. Modeling of alkali-silica reaction in concrete: a review. Front Struct Civ Eng 2012;6(1):1–18.

[47] El Mohandes F, Vecchio F. VecTor3: A. User’s Manual; B. Sample coupled thermal and structural analysis. Toronto, Canada: Dept. of Civil Engineering, University of Toronto; 2013.

[48] Rodriguez J, Lacoma Aller L, Martinez Cutillas F, Marti Rodriguez J. Contribution to Theme A of the benchmark workshop: effect of concrete swelling on the equilibrium and displacements of an arch dam. In: Proceedings of the XI ICOLD benchmark workshop on numerical analysis of dams, Valencia, Spain; 2011.

[49] Pan J, Feng Y, Jin F, Zhang C. Numerical prediction of swelling in concrete arch

dams affected by alkaliaggregate reaction. Eur J Environ Civ Eng 2013;17(4):231–47.
[50] Huang H, Spencer B. Grizzly model for fully coupled heat transfer, moisture, diffusion, alkali-silica reaction and fracturing process in concrete. In: Saouma V, Bolander J, Landis E, editors. 9th international conference on fracture mechanics of concrete and concrete structures; FraMCoS-9, Berkeley, CA; 2016. http://dx.doi.org/10.21012/FC9.194.
[51] Huang H, Spencer B, Cai G. Grizzly model of multi-species reactive diffusion, moisture/heat transfer, and alkali-silica reaction in concrete. Tech. Rep. INL/EXT-15-36425. Idaho Falls, Idaho 83415: Idaho National Laboratory; 2015.
[52] Ben-Ftima M, Sadouki H, Bruhwiler E. Development of a computational multi-physical framework for the use of nonlinear explicit approach in the assessment of concrete structures affected by alklai-aggregate reaction. In: Saouma V, Bolander J, Landis E, editors. 9th international conference on fracture mechanics of concrete and concrete structures; FraMCoS-9, Berkeley, CA; 2016. http://dx.doi.org/10.21012/FC9.221.
[53] Capra B, Bournazel J. Modeling of induced mechanical effects of alkali-aggregate reactions. Cem Concr Res 1998;28(2):251–60.
[54] Saouma VE, Martin RA, Hariri-Ardebili MA, Katayama T. A mathematical model for the kinetics of the alkali–silica chemical reaction. Cem Concr Res 2015;68:184–95.
[55] Bryant L, Brokaw J, Mlakar P. Reliability modeling of concrete overstressing. Tech. Rep. JAYCOR, Vicksburg Mississippi, report Submitted to U.S. Army Engineer Waterways Experiment Station; 1993.
[56] Benjamin J, Cornell C. Probability, statistics, and decision for civil engineers. New York: McGraw Hill; 1970.
[57] Army Corps of Engineers. Reliability Assessment of Navigation Structures, ETL 1110-2-532. Washington, D.C.: Department of the Army, US Army Corps of Engineers; 1992.
[58] Army Corps of Engineers. Reliability assessment of navigation structures; stability of existing gravity structures, ETL 1110-2-321. Washington, D.C.: Department of the Army, US Army Corps of Engineers; 1993.
[59] Saouma V. Reliability based nonlinear fracture mechanics analysis of a concrete dam; a simplified approach. Dam Eng 2006;16(3):219–41.